Multiphase Dynamic Flash Simulations Using Entropy Maximization and Application to Compressible Flow with Phase Change

Lu Qiu, Yue Wang, and Rolf D. Reitz
Dept. of Mechanical Engineering, Engin Research Center, University of Wisconsin-Madison, 1500 Engineering Drive, Madison, WI 53706

DOI 10.1002/aic.14519
Published online June 16, 2014 in Wiley Online Library (wileyonlinelibrary.com)

A isochoric-isoenergetic flash solver using a direct entropy maximization principle for phase splitting and Gibbs free energy minimization for phase stability is developed. The solver searches for the global stable state in a rigorous and thermodynamically consistent way. The solver is demonstrated to be robust and efficient to handle multiphase flash, even in the vicinity of phase boundaries. Dynamic flash computations and gas dynamics simulations of shock waves are considered for pure ethylene and for binary ethylene-nitrogen mixtures. The simulations show significantly different shock wave characteristics when phase separation is considered due to intensive energy exchange, compared to the frozen flow limiting single-phase solution. © 2014 American Institute of Chemical Engineers *AIChE J*, 60: 3013–3024, 2014
Keywords: isoenergetic-isochoric flash, entropy maximization, phase transition, shock waves, two-phase flows

Introduction

Isochoric-isoenergetic (*UVn*) flash is a multiphase equilibrium calculation for which the system total internal energy (*U*), total volume (*V*), and mole numbers of each species (*n*) are specified but all other properties (e.g., the number of phases, phase composition) are to be determined. In industrial bath and distillation processing, careful monitoring of dynamic changes of a system state is crucial to process design and optimization. There has been a large amount of work focusing on the dynamic flash of distillation columns.[1–4] A thorough and excellent survey was made by Skogestad,[5] in which both basic dynamic flash algorithms and feedback-control methods are reviewed. Surprisingly, he found that there are almost no references on the *UVn* flash problem, although it is the direct and natural approach. Flatby et al.[6] concluded that commonly used steady-state distillation simulation packages use bubble-point type flash (which neglects vapor holdup[5]), but rigorous *UVn* flash (without any assumptions) is not widely used due to its complexity.

For computational fluid dynamics (CFD) simulations of two-phase flows, after solving the mass and energy equations, the thermodynamic state in each computational cell must be determined. When thermodynamic equilibrium is assumed, as in nearly all CFD solvers, consideration of the *UVn* flash is required. It is important to underline here that phase transition occurs if a multiphase state can further lower the system potential, based on fundamental thermodynamic principles. However, this has been generally overlooked in CFD solvers that use the ideal gas assumption, since the *UVn* flash is rather trivial because the internal energy is only a function of temperature, and pressure is directly calculated from the ideal gas relation. Indeed, rigorous *UVn* flash is challenging and there has been very limited research on this topic.

Correspondence concerning this article should be addressed to L. Qiu at lqiu4@wisc.edu

Literature Review

To our knowledge, all previous *UVn* flash calculations in the literature were performed using an equation of state (EOS) model applied to both the vapor and liquid phases. Saha and Carroll[7] used a nested loop method using the temperature, pressure and equilibrium ratios of each species as iterative variables to study the dynamic filling process. The outer isothermal-isobaric (*TPn*) flash was solved using an algorithm that is a combination of an accelerated successive substitution and the direct Newton method. This method, however, does not resolve numerical divergence because the initial guess needs to be carefully chosen and the step size carefully controlled. The initialization of temperature and pressure guesses is empirical and uses the pseudocritical properties. In addition, a switch to another type of flash (e.g., the isenthalpic-isobaric flash) is needed during the iterations. Michelsen[8] generalized flash calculation problems using thermodynamic state functions, and proposed two methods. For the first, the nested loop algorithm with the *TPn* flash was used in the inner loop to search for minimum locations of the state function, because this type flash is easier to handle using classical phase stability[9] and splitting[10] methods. This approach is similar to that of Saha and Carroll[7] because temperature and pressure are still used as the iterative variables. The second approach is to search for the saddle point, based on a modified objective function without

any constraints. This framework was later adopted by Goncalves et al.[11] They, however, noticed that convergence was very difficult to achieve or even was impossible, especially close to saturation points. Instead, the temperature, volumes of each phase, and mole numbers of each species were treated as independent variables. Later Lima et al.[12] took a different path to solve the *UVn* problem by solving both the differential and algebraic equations simultaneously using a differential equation solver called PSIDE. Compared with their previous treatment, a significant decrease in computation time was observed. However, this approach is not favored for CFD simulations as tracking the dynamic change of both thermodynamic and fluid dynamic properties is not practical. However, as long as the time step is small enough, a full separation of the thermodynamic and fluid dynamic calculation is reasonable. With this treatment, the thermodynamic state is determined from the fluid dynamics solution and the thermodynamic state is fixed during the fluid dynamic calculations. As a result, any EOS model can be applied to the thermodynamics modeling.

This point is also mentioned by Arendsen and Versteeg,[13] who considered the dynamic flash of a binary mixture of propane and *n*-butane in a liquefied gas tank. However, it was assumed that the number of phases was known *a priori* from calculated phase diagrams of internal energy and volume. However, this is not needed as a phase stability test can be used to verify if a single-phase mixture can exist. Their *UVn* problem then reduces solving different sets of algebraic equations, depending on whether the mixture is in the one- or two-phase state. A further extension work on pure carbon dioxide (CO_2) was recently presented by Giljarhus et al.[14] Dynamic simulation of a liquefied gas tank was performed, as well as a one-dimensional (1-D) pipe flow problem. For the fluid dynamic simulation, the solutions also captured the general structure of propagating waves. They further compared solutions with the stiffened gas and the Peng–Robinson EOS, and some discrepancies appeared for the predicted phase change in the depressurization process.

Castier[15] proposed a general scheme for solving the *UVn* flash problem using direct entropy maximization. He also proved that the widely used phase stability test[9] in traditional *TPn* flash calculations can be used directly when the temperature, pressure, and mole numbers are determined. As a result, a new phase is added only if the original tested mixture is not stable. His calculations show that the entropy maximization-based method is elegant and fast convergence is generally obtained in less than 10 iterations for two-phase flashes. In his work, the nested loop method based on *TPn* flash was also used, but the step size needed to be well-controlled to mitigate numerical instability. This is because a small variation of the temperature and pressure can lead to a dramatic change in thermodynamic properties, especially when the initial guesses are not good, and even phase change due to the phase stability test could occur. It was emphasized that the nested loop method was only used to get a coarse solution and if successful, the entropy maximization method would be activated.

In this article, several *UVn* flash problems are discussed. An entropy maximization-based *UVn* flash solver is developed, and it is validated with available literature data. Dynamic flash is also performed to monitor the state change of a system for further validation. The developed solver is then coupled with a fluid solver and CFD simulations of shock waves for pure ethylene and binary ethylene-nitrogen mixtures are performed.

Theory

For a specified thermodynamic system, the conservation laws give

$$\begin{cases} \dfrac{dn_i}{dt} = \sum\limits_{\text{in}} \dot{n}_i - \sum\limits_{\text{out}} \dot{n}_i \\ \dfrac{dU}{dt} = \sum\limits_{\text{in}} \dot{n}_i h_i - \sum\limits_{\text{out}} \dot{n}_i h_i + \dot{Q} \end{cases} \tag{1}$$

n_i is the number of moles of species i, h is the specific enthalpy, $\dot{Q}$ is the heat flux. Mass conservation is expressed using mole numbers because chemical reactions are not considered. In the energy equation, no extra work done by pressure is considered, as the system is rigid with constant volume. For a thermodynamic system, one explicit assumption is that the substances are perfectly mixed so the system is homogeneous. It is further assumed that thermodynamic equilibrium is attained instantaneously. Because the solution to Eq. 1 updates internal energy and mole numbers, thermodynamic equilibrium for such a system can be expressed in terms of entropy maximization[16] as

$$\text{maximize } S(U, V, \vec{n}) \text{ such that } \left(U^{\text{spec}}, V^{\text{spec}}, n_i^{\text{spec}}\right) \text{ is satisfied} \tag{2}$$

Here, U^{spec}, V^{spec}, and n_i^{spec} are the updated solutions from Eq. 1. Because of the involvement of the differential equation, Eq. 1, and the algebraic equation, Eq. 2, a system of differential-algebraic equations (DAEs)[1,6,11,12] is to be solved. Generally, there are two types of numerical methods to solve DAEs. The first is to solve simultaneously the DAEs, as used by Lima et al.[12] The second is to solve in a sequential manner, by first integrating the differential equations to get the internal energy, volume, and mole numbers, and then solving the algebraic equation. This method has been adopted by some researchers,[6,11] and is also used here.

UVn flash for mixtures

The most challenging problem in *UVn* flash computations for mixtures is the potential phase separation and recombination during dynamic evolution. As in the conventional *TPn* flash, we adopt a phase-wise method: First, we assume the mixture is single phase, and the phase stability is tested. If instability is detected, another phase is added and the equilibrium state is determined. This procedure continues until a global stable state is found. Formulated in this way, a new phase is only added if it increases the mixture entropy. For the phase stability, the classical tangent plane distance (TPD) method of Michelsen[9] was adopted. To solve for the TPD function, the general strategies suggested by Li and Firoozabadi[17] were used. More details on verification and example calculations for phase stability testing can be found in Ref. 18. Another type of stability test that considers given temperature, volume, and mole numbers has been developed recently by Mikyska and Firoozabadi[19,20] based on Helmholtz free energy minimization. Some advantages of using this type of stability test are discussed, and it is shown to provide great numerical efficiency.[20] However, the current *UVn* stability test seems to be most appropriate for the present problems of interest. Also, it is numerically easy and cheap to convert the *UVn* stability to the classical *TPn* stability (See section below about the *UVn* flash for single-phase mixture and discussions in Castier[15]).

For the phase splitting calculations, we adopted the method proposed by Castier[15] using direct entropy maximization. The dimensionless objective function is defined as

$$F_{\text{obj}} = -S\left(U, V, \vec{n}\right)/R_{\text{u}} \tag{3}$$

which is subject to the constraints

$$\begin{cases} \sum_j U_j = U^{\text{spec}} \\ \sum_j V_j = V^{\text{spec}} \\ \sum_j n_{ij} = n_i^{\text{spec}}, i = 1, ..., N_{\text{c}}, j = 1, ..., N_{\text{P}} \end{cases} \tag{4}$$

N_{c} and N_{P} are the numbers of components and phases, respectively. The following independent dimensionless and scaled variables are defined

$$\begin{cases} \alpha_j = U_j/U^{\text{spec}} \\ \beta_j = V_j/V^{\text{spec}} \\ \gamma_{ij} = n_{ij}/n_i^{\text{spec}} \end{cases} \tag{5}$$

A sizable number of thermodynamic properties and derivatives are needed to determine the Hessian matrix (e.g., $(\partial \ln(\varphi)/\partial T)_{v,\vec{x}}$, $(\partial \ln(\varphi)/\partial v)_{T,\vec{x}}$, and . $(\partial u/\partial v)_{T,\vec{x}}$) and more details can be found in the Appendix in Ref. 15. In the present simulations, the Peng–Robinson equation of state[21] (PR EOS) was used, as documented in Appendix, and all the derivatives needed are calculated analytically. A Newton-type second-order method[22] is applied to find the maximum entropy state. Changes to the Hessian matrix were made when necessary to ensure positive-definiteness and, hence, the convexity. A line search algorithm is then applied to determine the maximum step size along the descending direction. Our numerical experience has shown that this method is able to promote fast convergence, generally in less than 10 iterations. One special noteworthy feature is that the pressure can become negative during the iterations, which of course is an indication of an unstable mixture. However, when numerical convergence is achieved, the pressure will be positive and all the phases have the same temperature and pressure. Application of the above numerical algorithms on multicomponent mixture to study possible condensation occurring inside practical engine combustion chamber can be found in Qiu et al.[23] and Qiu and Reitz.[24]

UVn flash for single-phase mixture

When only a single-phase mixture is considered, although it may not be at a globally stable state, the *UVn* flash calculation is quite straightforward by solving

$$U = U^{\text{spec}} \tag{6}$$

Note that as an EOS model is used, the problem actually reduces to solving a nonlinear equation with a single unknown. Actually, it is the most basic type because the phase stability test is immediately followed once a feasible single-phase solution is found. Numerical experience shows that a classical Newton–Raphson iterative method can be used. It is further noticed that since the system is rigid, the derivative of molar internal energy with respect to temperature is in fact the constant volume specific heat.

UVn flash for pure species with phase change

When only one pure species is considered, the entropy maximization principle requires solving the following set of equations[14,25] for the two-phase state considering mechanical equilibrium, phase equilibrium, mass and energy conservation

$$\begin{cases} \lambda\rho_{\text{V}}u(T,P,Z_{\text{V}}) + (1-\lambda)\rho_{\text{L}}u(T,P,Z_{\text{L}}) = \rho^{\text{spec}}u^{\text{spec}} \\ \lambda = (\rho^{\text{spec}} - \rho_{\text{V}})/(\rho_{\text{V}} - \rho_{\text{L}}) \\ P = P^{\text{S}}(T) \\ f(T,P,Z_{\text{V}}) = f(T,P,Z_{\text{L}}) \end{cases} \tag{7}$$

λ is the volume fraction of the vapor phase; P^{s} is the saturation pressure of the pure species; ρ^{spec} is the specified density. The Newton–Raphson method can also be used very efficiently in this problem. One implementation of such algorithm to study two different condensation mechanisms for a pure species can be found in Qiu et al.[26,27]

Table 1. Component Properties and Non-Zero Interaction Parameters for Binary CH_4—H_2S Mixture

Species	T_{c} (K)	P_{c} (bar)	ω (−)	MW (g/mole)	k_{i,CH_4}	$k_{i,\text{H}_2\text{S}}$
CH_4	190.4	46.0	0.011	16		0.083
H_2S	373.2	89.4	0.081	34	0.083	

Results and Discussion

In the following presentations, the ideal gas properties (e.g., the constant pressure specific heat) were calculated using third-order polynomials and the coefficients can be found in Reid et al.[28] The reference state was taken at 298.15 K and 1 bar. Real gas properties were then determined using the corresponding departure functions.[29,30]

Validations of the UVn flash solver

The developed *UVn* flash solver was validated using the six problems found in Ref. 15, where all the specified inputs and initial guesses are presented. The first four problems are for binary CH_4-H_2S mixtures, and their properties are summarized in Table 1. The binary interaction parameter for this pair is 0.083.[15,31] The iteration histories of the present *UVn* solver are shown in Figure 1, and the final solutions are shown in Tables 2 and 3, along with Castier's solutions.[15] It is seen from the tables that our results agree well with his data. Some minor differences are believed to be due to slightly different species properties and/or EOS parameters used. The chemical potential μ is calculated through

$$\mu_i = \mu\left(T, P^0\right) + R_{\text{u}}\,T \ln\left(\frac{x_i \varphi P}{P^0}\right) \tag{8}$$

with P^0 the reference pressure. Since the chemical potential, which is the molar Gibbs free energy, always has a real value, it can be shown that the logarithm of the fugacity coefficient is the complex conjugate of the logarithm of pressure[32] when pressure is negative, as seen for Problem 1. It is also clear from Figure 1 that the two phases converge to same temperature and pressure on numerical convergence, consistent with the requirement of thermodynamic equilibrium.

The second mixture considered is a liquefied petroleum gas (LPG) mixture composed of six components.[15] The species thermodynamic properties are summarized in Table 4. The solutions are summarized in Table 5, and the iterations are shown in Figure 2. As before, our results are identical to the solutions found in Ref. 15. The global phase diagram for the LPG mixture in pressure-temperature space was constructed

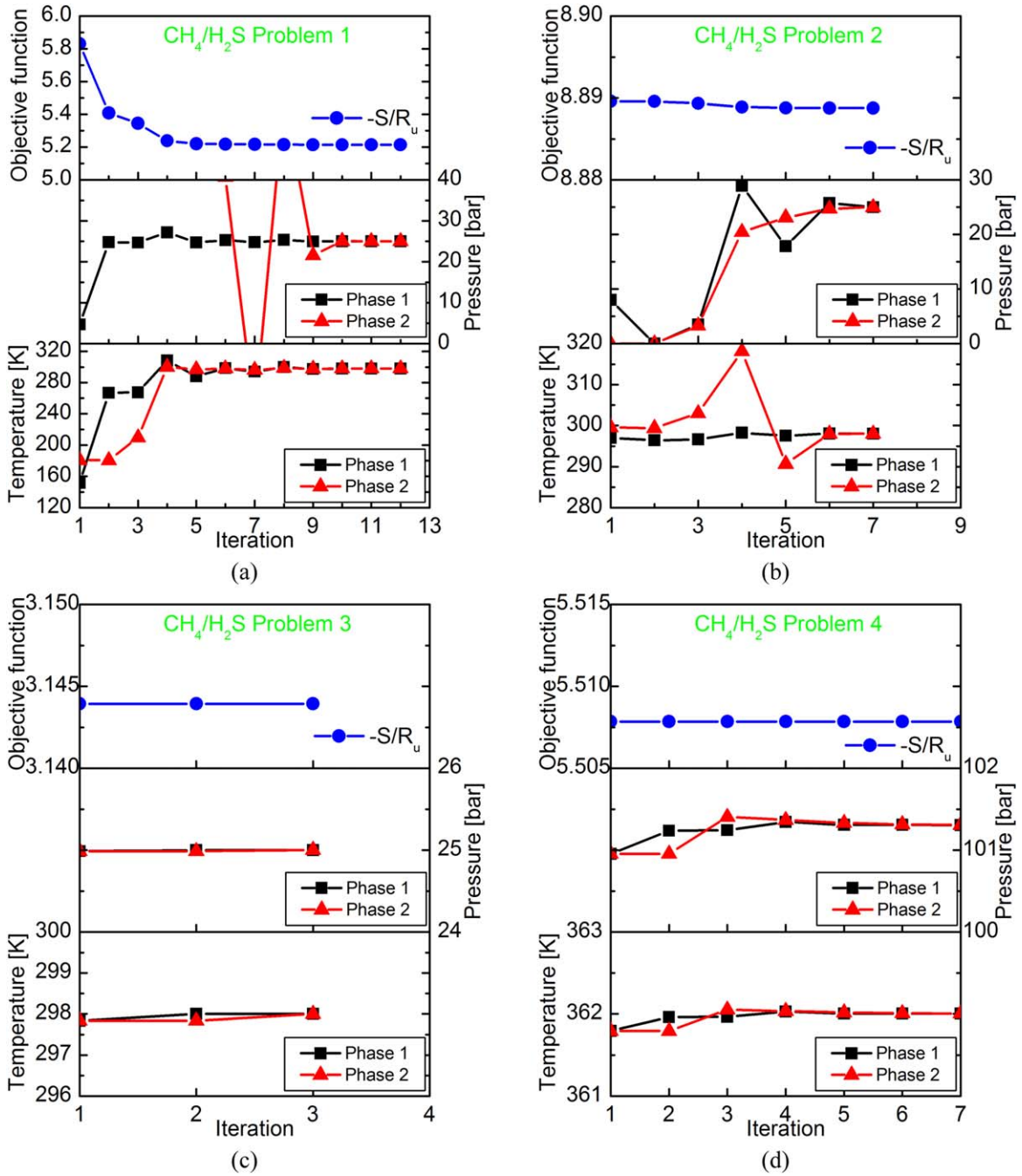

Figure 1. Iteration histories of temperature, pressure, and the objective function for binary CH_4/H_2S mixture.

(a) Problem 1. (b) Problem 2. (c) Problem 3. (d) Problem 4. [Color figure can be viewed in the online issue, which is available at wileyonlinelibrary.com.]

Table 2. Final Solutions of Problems 1 and 2 for Binary CH_4—H_2S Mixture

	Problem 1				Problem 2			
	Vapor Phase		Liquid Phase		Vapor Phase		Liquid Phase	
	Present	Castier's	Present	Castier's	Present	Castier's	Present	Castier's
Internal energy (J)	−211,515.2	−211,515.6	−544,985.5	−544,985.2	−424.4	−424.4	−1,510,983.3	−1,510,983.3
Volume (cm^3)	51,366.7	51,367.2	1502.26	1502.25	103.06	103.07	4165.04	4165.03
Moles of CH_4	9.6643	9.6643	0.3357	0.3357	0.0194	0.0194	0.9306	0.9306
Moles of H_2S	54.314	54.314	35.686	35.6860	0.1090	0.1090	98.941	98.941
Compressibility factor	0.81015	0.81016	0.04208	0.04208	0.81016	0.81016	0.04208	0.04208
T [K]	298.0	298.0	298.0	298.0	298.0	298.0	298.0	298.0
P [bar]	25.0	25.0	25.0	25.0	25.0	25.0	25.0	25.0

Table 3. Final Solutions of Problems 3 and 4 for Binary CH_4—H_2S Mixture

	Problem 3				Problem 4			
	Vapor Phase		Liquid Phase		Vapor Phase		Liquid Phase	
	Present	Castier's	Present	Castier's	Present	Castier's	Present	Castier's
Internal energy (J)	−330,473.1	−330,473.1	−610.6	−610.6	−38,792.7	−385,295.5	−248,540.99	−251,172.5
Volume (cm^3)	80,256.42	80,256.43	1.68	1.68	6383.32	6352.52	3543.39	3574.19
Moles of CH_4	15.0996	15.1000	0.00376	0.00038	6.4171	6.3857	3.5829	3.6143
Moles of H_2S	84.860	84.860	0.03998	0.03998	56.046	55.711	33.95	34.289
Compressibility factor	0.81016	0.81016	0.04208	0.04208	0.34398	0.34432	0.3177	0.31739
T [K]	298.0	298.0	298.0	298.0	362.0	362.0	362.0	362.0
P [bar]	25.0	25.0	25.0	25.0	101.3	101.3	101.3	101.3

Table 4. Component Properties for the LPG Mixture

Species	Composition	T_c (K)	P_c (bar)	ω (−)	MW (g/mole)
C_2H_6	0.01080	305.4	48.8	0.099	30.0
C_3H_6	0.36080	364.9	46.0	0.144	42.0
C_3H_8	0.14650	369.8	42.5	0.153	44.0
iC_4H_{10}	0.23300	408.2	36.5	0.183	58.0
nC_4H_{10}	0.23300	425.2	38.0	0.199	58.0
nC_5H_{12}	0.01590	469.7	33.7	0.251	72.0

Table 5. Final Solutions of Problems 5 and 6 for the LPG Mixture

	Problem 5				Problem 6			
	Vapor Phase		Liquid Phase		Vapor Phase		Liquid Phase	
	Present	Castier's	Present	Castier's	Present	Castier's	Present	Castier's
Internal energy (J)	−37,9828.1	−37,9827.4	−1,589,2678.3	−1,589,2679.0	177,582.2	177,502.2	−15,2225.2	−15,2643.9
Volume (cm^3)	401,207.01	401,206.90	78,637.99	78,638.07	272,958.33	272,894.49	16,441.67	16,485.86
Moles of C_2H_6	4.2035	4.2035	6.5965	6.5965	10.055	10.053	0.74499	0.74702
Moles of C_3H_6	68.223	68.223	292.58	292.58	333.35	333.28	27.451	27.525
Moles of C_3H_8	24.416	24.416	122.08	122.08	135.18	135.15	11.324	11.354
Moles of iC_4H_{10}	18.527	18.527	214.47	214.47	213.40	213.35	19.595	19.648
Moles of nC_4H_{10}	13.884	13.884	219.12	219.12	212.85	212.8	20.150	20.204
Moles of nC_5H_{12}	0.31554	0.32554	15.574	15.574	14.371	14.366	1.5295	1.5335
Compressibility factor	0.86897	0.86897	0.02536	0.02536	0.38249	0.38249	0.26212	0.26212
T [K]	300.0	300.0	300.0	300.0	395.0	395.0	395.0	395.0
P [bar]	7.0	7.0	7.0	7.0	42.3	42.3	42.3	42.3

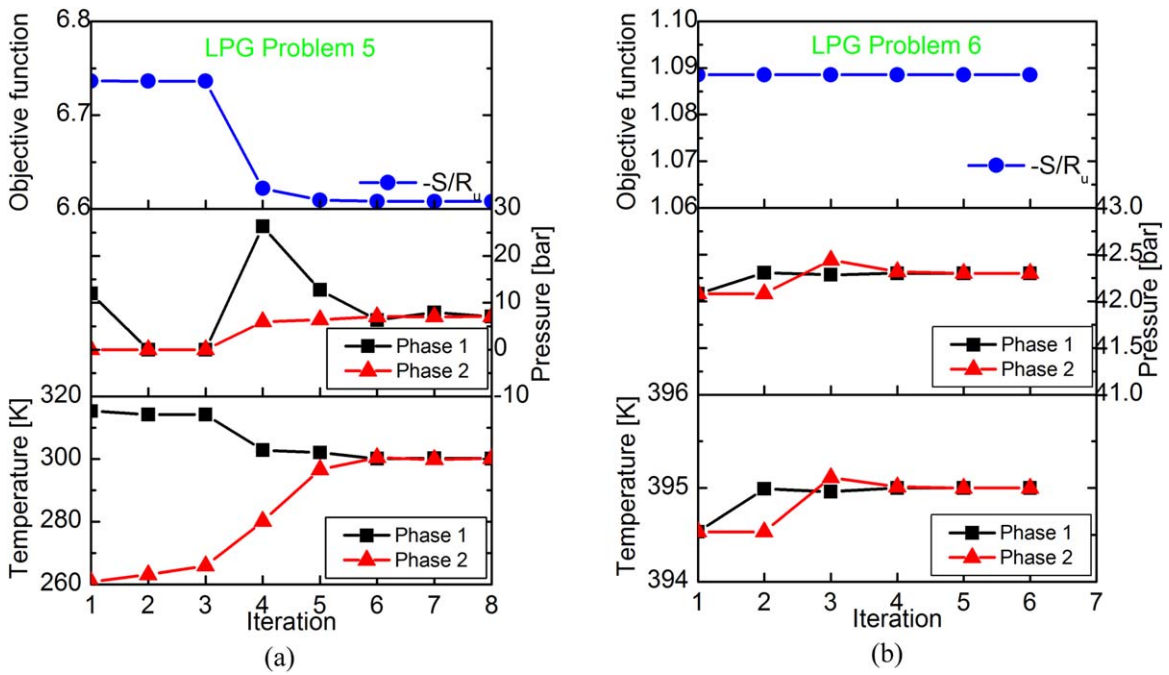

Figure 2. Iteration histories of temperature, pressure, and the objective function for the LPG mixture.

(a) Problem 5. (b) Problem 6. [Color figure can be viewed in the online issue, which is available at wileyonlinelibrary.com.]

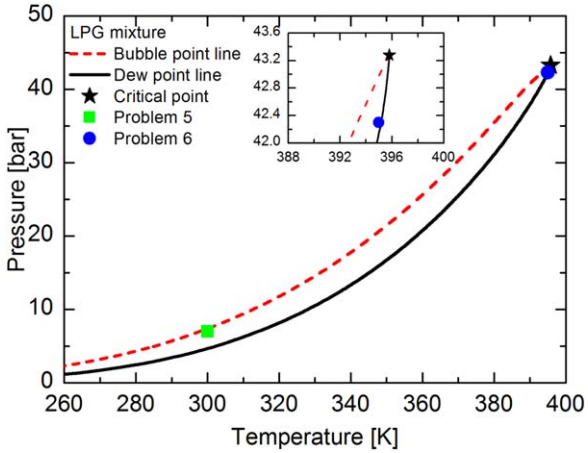

Figure 3. Pressure-temperature phase diagram of the LPG mixture (six components).

Also shown are the solution of Problem 5 and 6 the critical point. [Color figure can be viewed in the online issue, which is available at wileyonlinelibrary.com.]

using *TPn* flash,[18] as shown in Figure 3. (The phase boundary is determined if a phase appears or disappears by varying the pressure by 0.01 bar.) Saha and Carroll[7] and Goncalves et al.[11] pointed out that the most time-expensive and difficult calculations are in the vicinity of the critical point and near the saturation line. The critical point is (395.8 K, 43.28 bar). However, the above calculations show that our entropy maximization method does not have this issue.

Dynamic flash of C_2H_4—N_2

Dynamic flash simulations were performed for binary mixtures of C_2H_4 and N_2 and their critical properties are shown in Table 6. The interaction parameter for this pair is 0.051.[33] Figure 4 shows a comparison between the predicted results using vapor-liquid equilibrium (VLE) and experimental data,[34,35] and a good match is observed.

The vessel is initially at 200 K and 1 bar with 100 moles of C_2H_4 and N_2 each. There is a well-controlled continuous input stream of 10 mole/s (with C_2H_4:N_2 = 0.8:0.2 (mole)) at 250 K and 50 bar. Notice that the input stream is in a two-phase state. The evolution of the system is shown in Figure 5. The system was initially in the vapor phase, and this state

Table 6. Component Properties and Non-Zero Interaction Parameters for C_2H_4 and N_2

Species	T_c (K)	P_c (bar)	ω (−)	MW (g/mole)	k_{i,C_2H_4}	k_{i,N_2}
C_2H_4	282.34	50.41	0.0862	28.053		0.051
N_2	126.2	33.9	0.0377	28.013	0.051	

lasted only about 17 s. During this period, the system temperature decreased but pressure increased due to filling with the high-pressure fluid. After entering the two-phase state, the vapor phase volume fraction keeps decreasing. It decreases slowly at early times, but faster at late times until the two-phase stage ends. The temperature and pressure then start to increase. The mole fraction of C_2H_4 is larger than that of N_2 in both the vapor and liquid phases. At around 4180 s, the two-phase state terminates as the liquid phase builds up and the system evolves into a single-phase state. This state has a vapor-like compressibility factor at high temperature and pressure. Discontinuities in the slopes of both the temperature and pressure profiles are observed when the system changes from a single-phase to a two-phase state, or vice versa. For the pressure, its slope of change is larger when entering into the single-phase state than that when entering the two-phase region. Due to nonlinear effects in the phase change processes, curvature is observed in the profiles of temperature, pressure, and compressibility factors.

Shock waves in pure C_2H_4

The validated *UVn* flash solver was coupled with a fluid solver to perform fluid dynamics simulations. The open-source CFD code KIVA-3V Release 2[36] was used, which has been widely applied for multidimensional diesel spray combustion simulations.[37] As the standard KIVA code uses the ideal gas relation, the thermodynamic relationship was generalized using the PR EOS and the details can be found in Trujillo et al.[38] and Qiu et al.[23]

A 1-D simulation was performed for pure C_2H_4 in a tube of length of 20 cm, and 1000 grid points were used. Pressure inflow and outflow boundary conditions were applied at the left and right ends, respectively. Initially, the tube was at 50 bar and 260 K, and the depressurizing process was modeled by enforcing a pressure of 20 bar at the right hand end at $t = 0$. Simulation results are shown in Figures 6 and 7 at

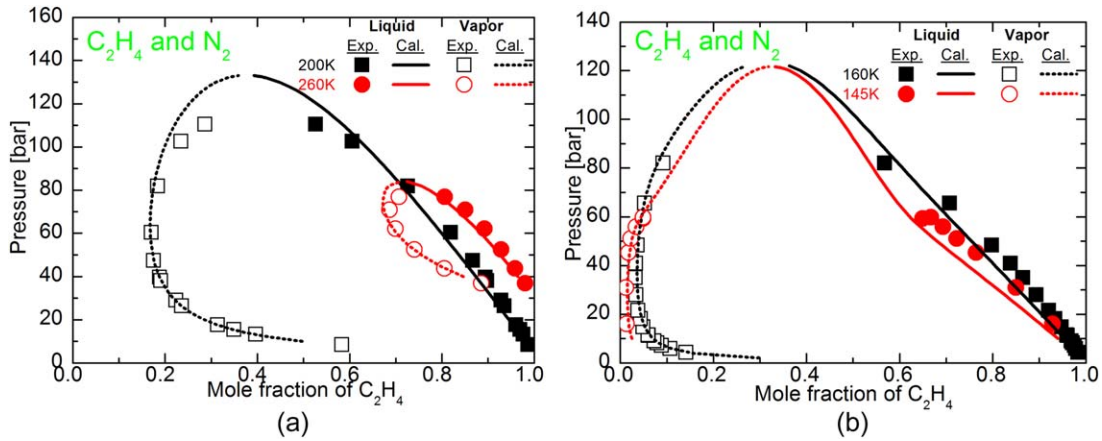

Figure 4. Vapor-liquid equilibrium of binary C_2H_4—N_2 mixtures (a) at two lower temperatures and (b) at two higher temperatures.

[Color figure can be viewed in the online issue, which is available at wileyonlinelibrary.com.]

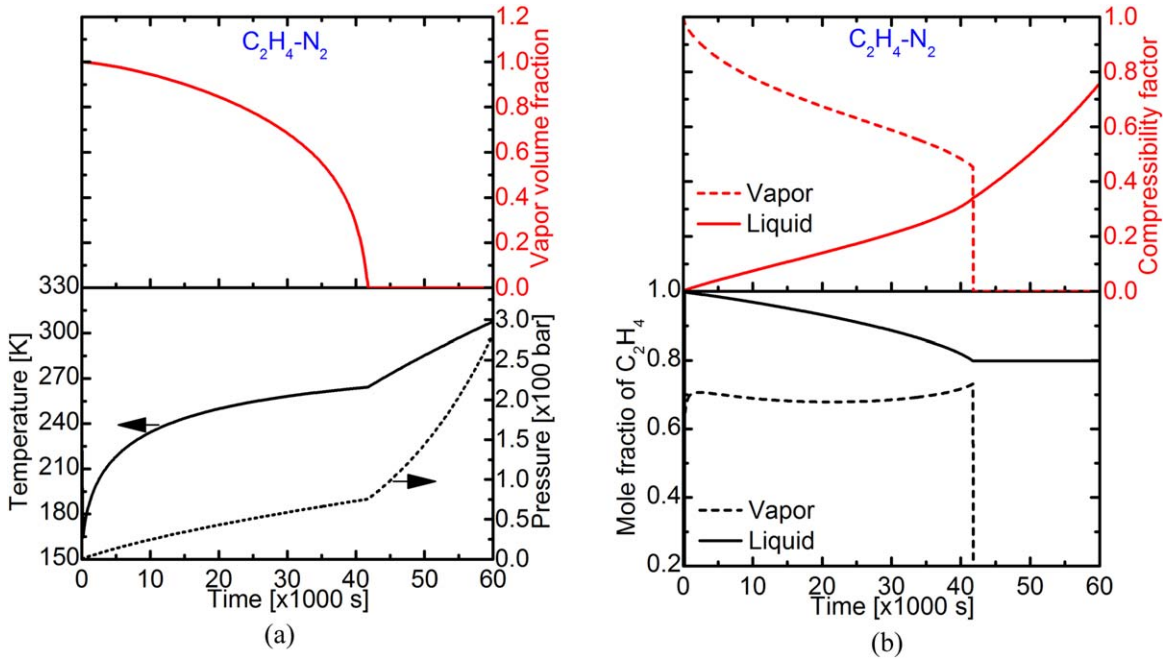

Figure 5. Dynamic evolution of the properties for the tank filled with C_2H_4—N_2 mixtures.

(a) Vapor volume fraction, temperature, and pressure. (b) Compressibility factor and mole fraction of C_2H_4 in each phase. [Color figure can be viewed in the online issue, which is available at wileyonlinelibrary.com.]

different times. With pressure release, a pressure wave is seen to propagate to the left due to the expansion, as seen in the profiles in Figure 6 at $t = 0.1$ and 0.3 ms, respectively. Two kinds of simulation were considered. The first simulation only considered single-phase gas dynamics with real gas effects. However, the general shapes of the profiles of this simulation are similar to solutions obtained using the ideal gas law, but it is more accurate as it considers departures from an ideal gas. As the fluid is in the compressed liquid state, the small compressibility factor indicates strong nonideality. In the second simulation, phase equilibrium was activated with possible two-phase solutions, which can be considered as the true thermodynamic solution with phase separation. All the discontinuities across the shocks are seen to be well captured for both the single-phase and two-phase solutions. Figures 6c, d show that the liquid volume fraction drops at the right end of the tube after the depressurizing event, which is an indication of an evaporation process. This phase separation process creates a shock wave-like discontinuity in the fluids due to the sudden energy absorption. An "inverse" condensation process due to supersaturation of the vapor phase is seen, which has been termed a "condensation shock" when the associated heat release leads to discontinuity in the slope of the pressure profiles.[39] More appropriately, the present discontinuity due to phase change is a "thermodynamic shock" because it distinguishes a change in thermodynamic state from the single-phase state to a two-phase state through an intensive energy interaction process. In contrast to the single-phase solutions, the direct consequence of the evaporative "cooling" effect is that the temperature drops while the pressure increases.

Results at two later times (1.5 and 1.8 ms) are shown in Figure 7, when the rarefaction wave has already touched the left inflow boundary and is reflecting back. When the wave entered the two-phase region at the right hand end, the liquid phase increased and a sharp liquid volume fraction gradient was observed, as shown in Figure 7c. Because of the condensation, there was a bump in the pressure profile and a strong gradient in the temperature profile, as expected due to the aforementioned thermodynamic shock. The single-phase simulation generally underestimated the pressure due to the neglect of the phase-change-induced shock appearing in the two-phase simulation. At $t = 1.8$ ms, the wave is reflected to the left. For the single-phase simulation, because of the higher sound speed in the liquid phase, the wave travels faster compared to that from the two-phase simulation, in which the sound speed is significantly reduced in the two-phase region, as seen in Figure 7b. At the same time, as the shock wave leaves the two-phase region, Figure 7d shows that the gradient of liquid volume fraction is elevated and the two-phase region is transported to the left, but its velocity is relatively low.

In summary, there are two interesting observations. First, the single-phase solution shows two pressure plateaus, as in classical gas dynamics. For the two-phase solution, because of the phase-change-induced thermodynamic shock, one pressure plateau is in the vapor pressure, which separates the regions of high and low pressures, as also seen in Ref. 14. In addition, the region between the vapor pressure and lower pressure is also a two-phase region. The temperature profile for the two-phase solution has a similar three-stepped profile as for the pressure. However, the single-phase solution has temperature plateaus at the higher temperature, and the lower temperature is close to the saturation temperature. Second, as the two-phase simulation gives the correct solutions satisfying thermodynamic equilibrium unconditionally, and they are very different from the results from simulations limited to only one phase, consideration of phase change is believed to be critically needed in simulating these two-phase flows.

Shock wave in C_2H_4 and N_2 mixture

Finally, shock waves in a binary mixture of C_2H_4 and N_2 were also considered. The general setup was the same as in Shock waves in pure C_2H_4 section above. Initially, the left

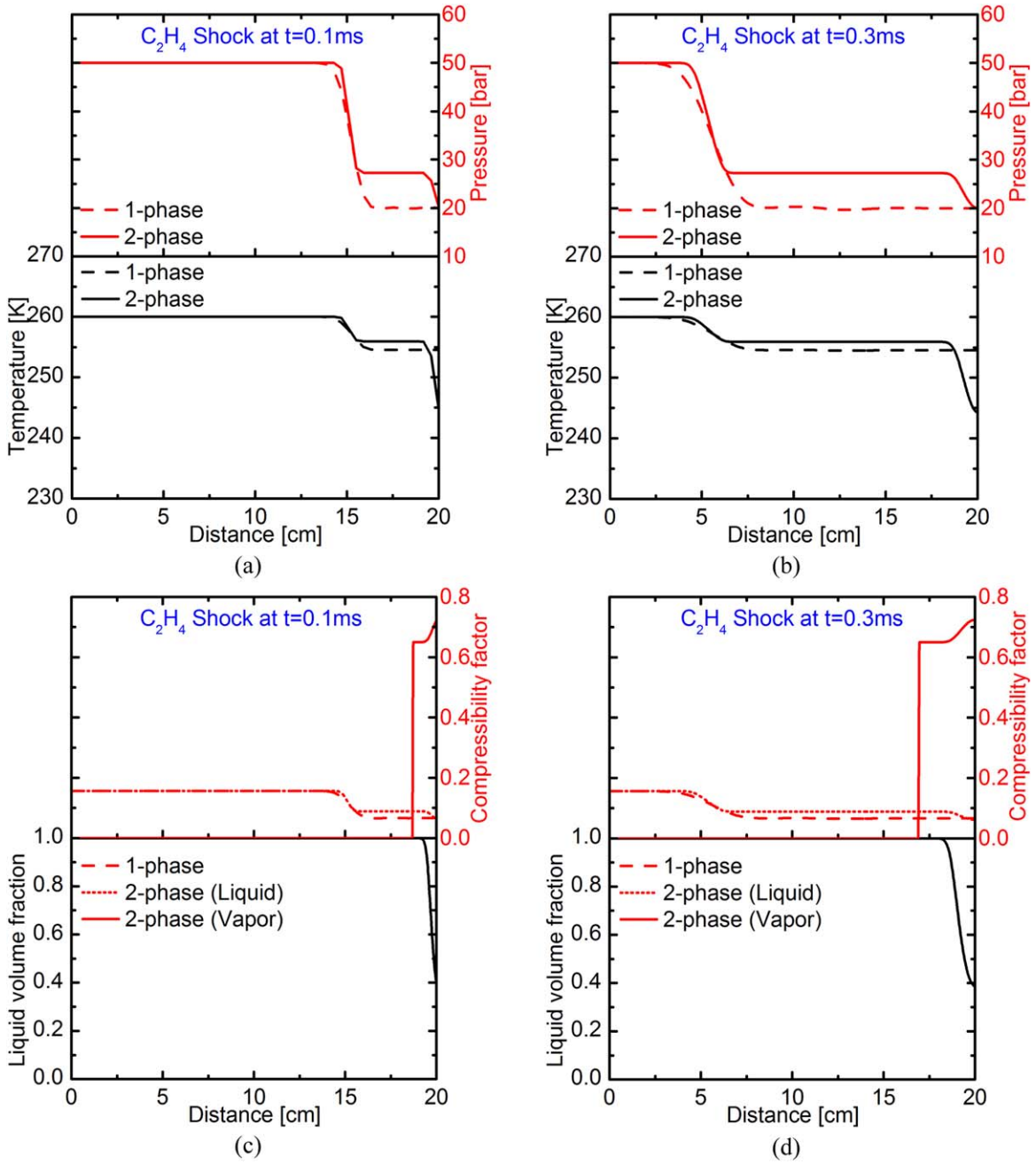

Figure 6. Shock tube simulation of the pure C_2H_4 at early times.

(a) and (c): Temperature, pressure, compressibility factor, and liquid volume fraction at $t = 0.1$ ms. (b) and (d): Temperature, pressure, compressibility factor, and liquid volume fraction at $t = 0.3$ ms. "1-phase" stands for single-phase solution without phase change and "2-phase" stands for two-phase solution considering phase equilibrium. [Color figure can be viewed in the online issue, which is available at wileyonlinelibrary.com.]

section of the tube was filled with C_2H_4 at (300 K, 50 bar) while the other half (the right section) was filled with N_2 at (180 K, 40 bar). Therefore, both species are initially at supercritical states with respect to their own critical points. Once the diaphragm is released, a rarefaction wave moves toward the left while a compression wave moves to the right. After touching the boundary, the previously left running wave is reflected to the right at the inflow boundary and it forms a "left reflected wave." Conversely, the previously right running wave is reflected toward the left at the outflow boundary as a "right reflected wave." The simulation results show that phase change is not observed to occur until 0.71 ms, when the right reflected wave meets the contact surface. Physically, this is because the pressure wave acts as a compression force in the mixing region and the mixture is brought back into the two-phase region and condensation occurs.

To better show the phase transition process, simulation results are presented in Figure 8 at six different times. The first three time instants show the compression waves while the latter three show the expanding waves. Figure 8a shows that the two reflected waves are about to meet, as observed from the change of the number of discontinuities from $t = 0.71$ to 0.75 ms. The contact surface can be seen from the vapor phase compressibility factor profile in Figure 8c. The frozen Mach number is the mass averaged Mach number of the liquid and vapor phases. It is remarked that the

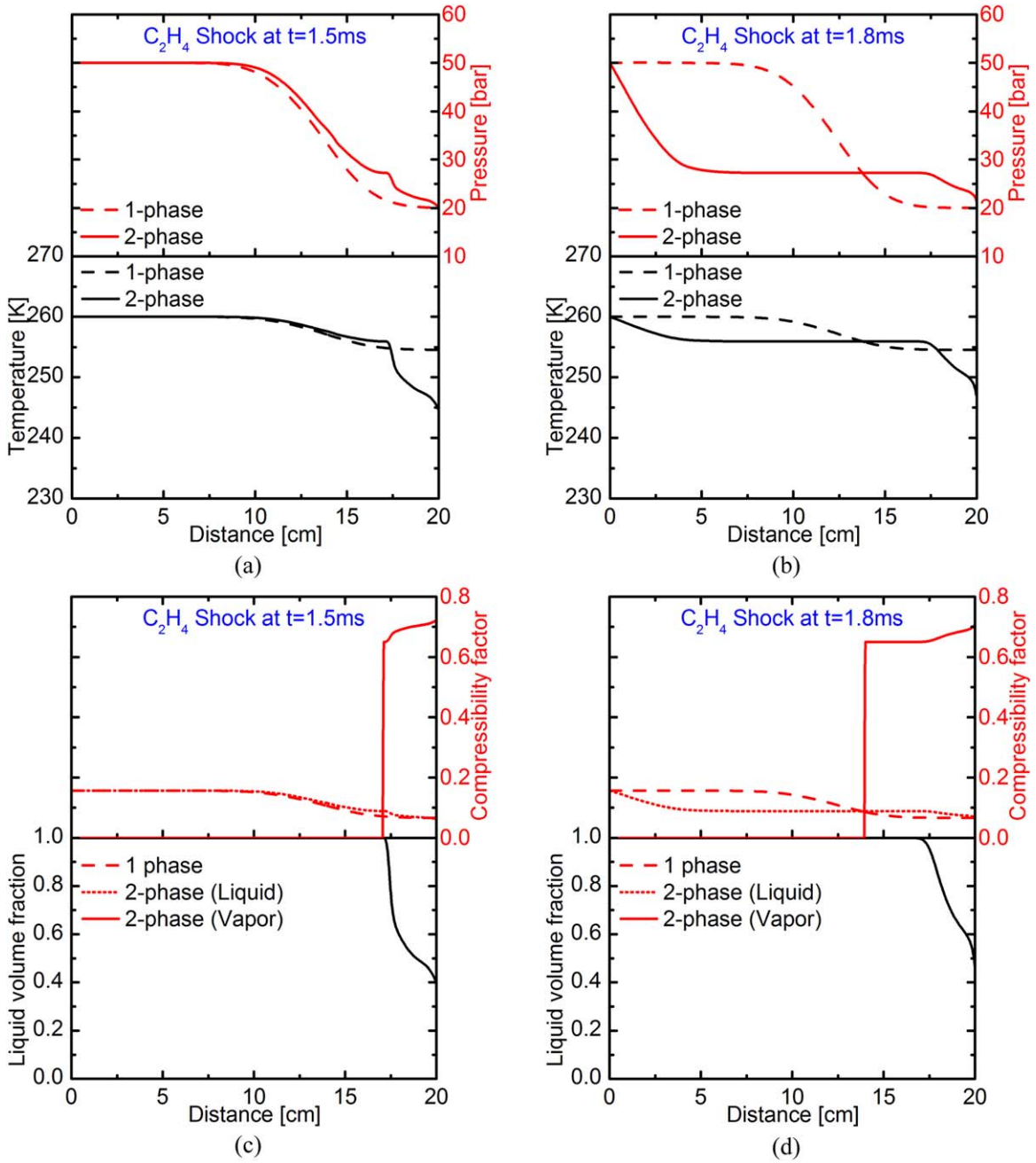

Figure 7. Shock tube simulation of the pure C_2H_4 at later times.

(a) and (c): Temperature, pressure, compressibility factor, and liquid volume fraction at $t = 1.5$ ms. (b) and (d): Temperature, pressure, compressibility factor, and liquid volume fraction at $t = 1.8$ ms. [Color figure can be viewed in the online issue, which is available at wileyonlinelibrary.com.]

thermodynamically true sound speed of a two-phase mixture can be determined according to the method proposed by Pan and Firoozabadi,[40] Nichita et al.,[41] and Castier,[42] based on the thermodynamic definition of the isentropic sound speed. As a result, the sound speed based on the "frozen flow" is continuous, but the actual thermodynamically correct sound speed exhibits a discontinuity across the phase border. This is well shown by the bumps in the frozen Mach number plots.

Figures 8b, d show the simulation results at three time instants after the meeting event between the reflected wave and the contact surface. It is observed that the two waves now leave the contact surface, especially from the temperature and Mach number plots. Compared to the Mach numbers in Figures 8c, d, it is noticed that the flow is actually accelerated due to compression. The phase separation continues until after 0.8 ms when no bumps are seen in the Mach number profile. For a more direct comparison, Figures 9a, b show the evolution of the liquid phase volume fraction and liquid compressibility factor in this period, respectively. It is noticed that condensation occurs in the small mixing region and the two-phase mixture is transported downstream along with the contact surface. The newly formed liquid phase disappears when the pressure wave expands and leaves the mixing region. Therefore, the phase transition only occurs during the period which starts from the instant when the right reflected wave touches the contact surface to the instant when they separate. The nascent liquid phase lasts for around 0.9 ms starting from 0.71 to 0.8 ms, and the largest

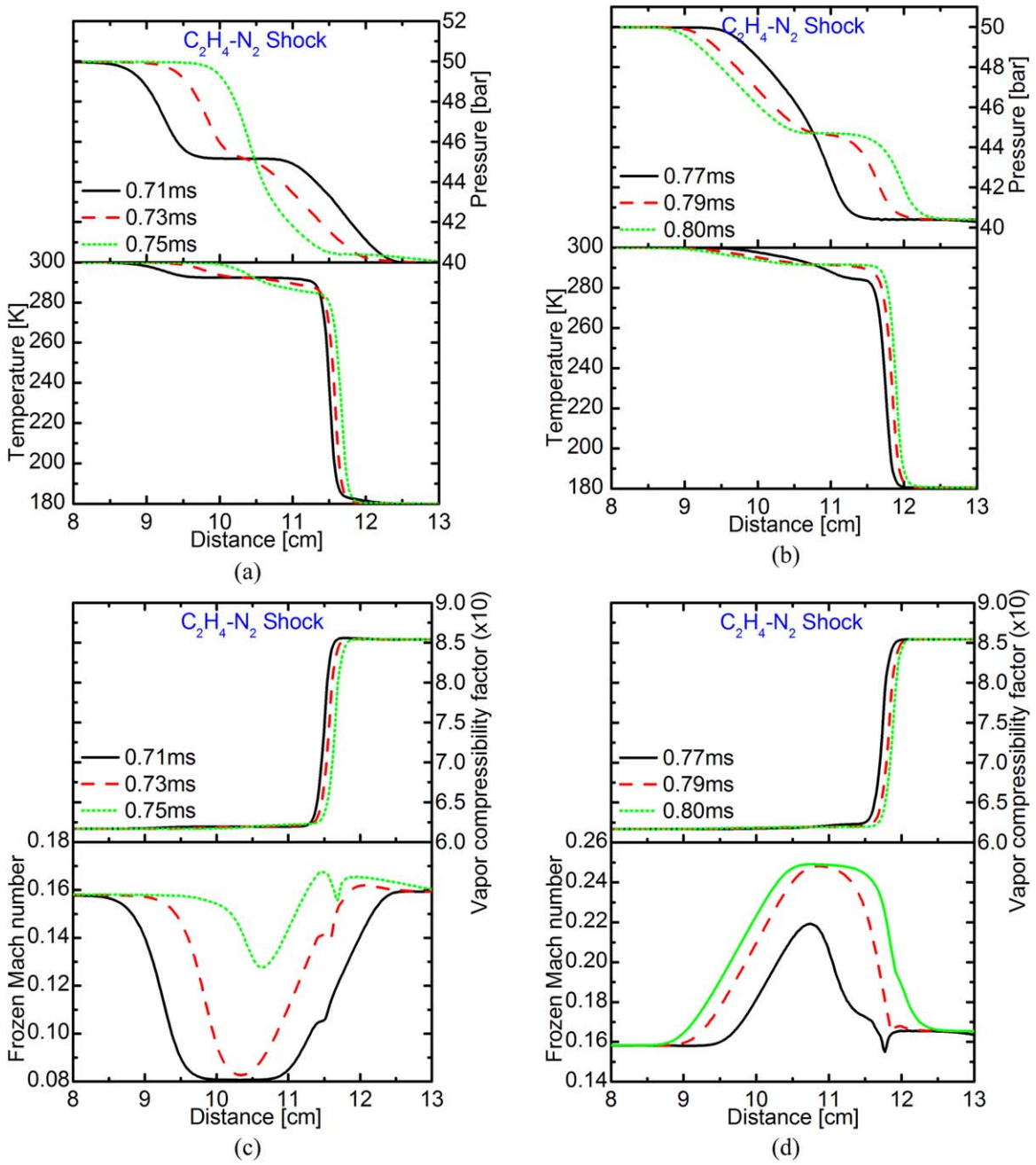

Figure 8. Shock tube simulation results of binary C_2H_4—N_2 mixture.

(a) and (c): Temperature, pressure, vapor compressibility factor and frozen Mach number at $t = 0.71$, 0.73, and 0.75 ms. (b) and (d): Temperature, pressure, vapor compressibility factor, and frozen Mach number at $t = 0.77$, 0.79, and 0.8 ms. "Frozen Mach number" is the mass averaged Mach number of the two phases. Note that the vapor compressibility factor is enlarged by 10 times and domain is limited to between 8 and 13 cm. [Color figure can be viewed in the online issue, which is available at wileyonlinelibrary.com.]

liquid volume fraction is about 1.4% at $t = 0.77$ ms. In this problem, the liquid volume fraction is rather small, so the energy released during the process is not large enough to promote a strong thermodynamic shock, as was observed in Shock waves in pure C_2H_4 section for the pure ethylene case, so the energy cascade is not too intensive, and no obvious discontinuity appears in the temperature and pressure profiles.

Summary and Conclusions

To study phase transition processes in compressible flows, both 0-D dynamic flash computations and 1-D gas dynamics simulations were performed using the PR EOS applied to both vapor and liquid phases. A *UVn* flash solver based on the entropy maximization principle was developed and validated using literature results. Further, its application to model two-phase flows was demonstrated in dynamic flash and CFD simulations on pure ethylene and binary ethylene-nitrogen mixtures.

For the 0-D dynamic flash problem, phase change processes in a constant-volume vessel were considered. One-dimensional computational fluid dynamics simulations were used to validate the coupling of the flash solver with a fluid solver. Appreciable differences were observed between simulations considering and not considering phase transitions, especially when the phase change was large enough to

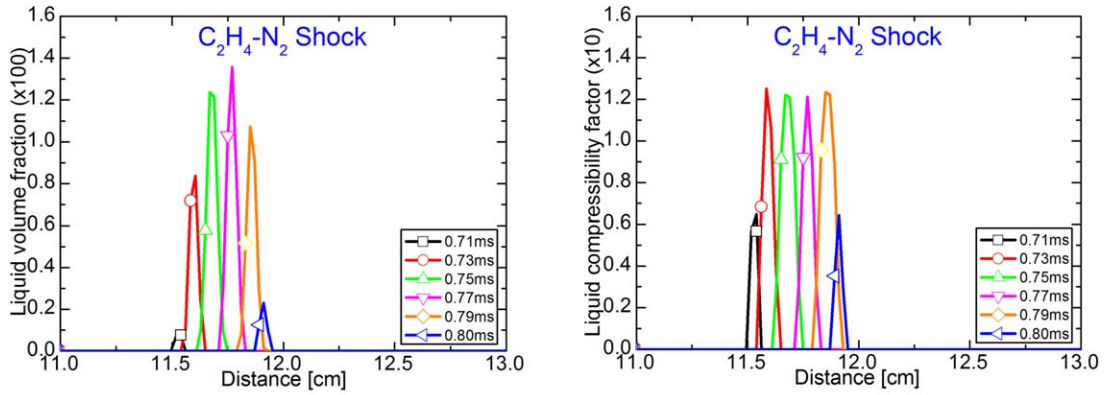

Figure 9. Phase transition process of the binary C_2H_4—N_2 mixture from 0.71 to 0.8 ms.

(a): Evolution of liquid volume fraction. (b) Evolution of liquid phase compressibility factor. Liquid volume fraction and liquid compressibility factor are enlarged by 100 and 10 times, respectively. Domain is limited to between 11 and 13 cm. [Color figure can be viewed in the online issue, which is available at wileyonlinelibrary.com.]

promote shock wave-like discontinuities in the pressure profiles. Specifically for a pure species shock wave experiencing evaporation, high and low pressure regions were found to be separated by the saturation pressure, and a large amount of liquid phase was converted to the vapor phase. For the binary mixture shock wave problem, condensation did not occur until the right reflected wave touched the mixing region, where compression effects led the mixture into the two-phase region and phase separation took place. Condensation was predicted to continue until the reflected waves left the contact surface as the pressure started to drop with the expanding wave, and hence, the amount of liquid phase was decreased.

Acknowledgments

The research work was conducted at the Engine Research Center and sponsored by Department of Energy and Sandia National Laboratories through the Advanced Engine Combustion Program (MOU 04-S-383) under the management of Dr. Dennis L. Siebers. Lu Qiu would like to thank Professor Marcelo Castier at the TAMU at Qatar for helpful and insightful communications on the entropy maximization method.

Notation

a = energy parameter in Eq. A1
a_i = energy parameter for component i in Eq. A4
a_{ij} = energy parameter between component i and j in Eq. A4
b_i = volume parameter for component i in Eq. A4
b = volume parameter in Eq. A1
F = the objective function in Eq. 3
h = specific enthalpy, J/mol
n_i = mole number of component i, mol
n_{ij} = mole number of component i in phase j, mol
n = mole number, mol
N_c = number of components
N_P = number of phases
P = pressure, bar
$\dot{Q}$ = heat transfer rate, W
R_u = universal gas constant, 8.314 J/mol-K
S = entropy, J/K
T = temperature, K
u = specific internal energy, J/mol
U = internal energy, J
v = specific molar volume, m^3/mole
V = volume, m^3
x_i = mole fraction of component i
Z = compressibility factor

Greek letters

α = parameter in Eq. A2
α_j = scaled internal energy for phase j
β_j = scaled volume for phase j
γ_{ij} = scaled mole numbers for component i in phase j
$\delta_{i,j}$ = binary interaction parameter between component i and j
κ = parameter in Eq. A3
λ = vapor phase volume fraction
μ = chemical potential, J/mole
ρ = density, kg/m^3
φ = fugacity coefficient
ω = acentric factor

Subscripts

c = critical property
L = liquid phase
V = vapor phase

Superscripts

0 = ideal gas
obj = the objective function
spec = specified value
s = saturation state of a pure species

Abbreviations

CFD = computational fluid dynamics
EOS = equation of state
PR = Peng–Robinson
MW = molar weight, g/mole
TPD = tangent plane distance
TPn = isothermal-isobaric flash
UVn = isoenergetic-isochoric flash
DAE = differential and algebraic equation
VLE = vapor-liquid equilibrium
0-D = zero-dimensional
1-D = one-dimensional

Literature Cited

1. Gani R, Ruiz CA, Cameron IT. A generalized model for distillation columns—I: model description and applications. *Comput Chem Eng*. 1986;10(3):181–198.
2. Cameron IT, Ruiz CA, Gani R. A generalized model for distillation columns—II: numerical and computational aspects. *Comput Chem Eng*. 1986;10(3):199–211.

3. Alejski K, Duprat F. Dynamic simulation of the multicomponent reactive distillation. *Chem Eng Sci*. 1996;51(18):4237–4252.
4. Pilavachi PA, Schenk M, Perez-Cisneros E, Gani R. Modeling and simulation of reactive distillation operations. *Ind Eng Chem Res*. 1997;36(8):3188–3197.
5. Skogestad S. Dynamics and control of distillation columns—a critical survey. *Model Ident Control*. 1997;18(3):177–217.
6. Flatby P, Skogestad S, Lundstrom P. *Rigogous Dynamic* S*imulation of Distillation Columns Based on UV-Flash*. In: IFAC Symposium ADCHEM'94. Kyoto, Japan, 1994.
7. Saha S, Carroll JJ. The isoenergetic-isochoric flash. *Fluid Phase Equilibr*. 1997;138(1–2):23–41.
8. Michelsen ML. State function based flash specifications. *Fluid Phase Equilibr*. 1999;158:617–626.
9. Michelsen ML. The isothermal flash problem.1. *Stability*. *Fluid Phase Equilibr*. 1982;9(1):1–19.
10. Michelsen ML. The isothermal flash problem.2. *Phase-split calculation*. *Fluid Phase Equilibr*. 1982;9(1):21–40.
11. Goncalves FM, Castier M, Araujo OQF. Dynamic simulation of flash drums using rigorous physical property calculations. *Braz J Chem Eng*. 2007;24(2):277–286.
12. Lima ERA, Castier M, Biscaia EC. Differential-algebraic approach to dynamic simulations of flash drums with rigorous evaluation of physical properties. *Oil Gas Sci Technol*. 2008;63(5):677–686.
13. Arendsen ARJ, Versteeg GF. Dynamic thermodynamics with internal energy, volume, and amount of moles as states: application to liquefied gas tank. *Ind Eng Chem Res*. 2009;48(6):3167–3176.
14. Giljarhus KET, Munkejord ST, Skaugen G. Solution of the Span–Wagner equation of state using a density–energy state function for fluid-dynamic simulation of carbon dioxide. *Ind Eng Chem Res*. 2012;51(2):1006–1014.
15. Castier M. Solution of the isochoric-isoenergetic flash problem by direct entropy maximization. *Fluid Phase Equilibr*. 2009;276(1):7–17.
16. Callen HB. Thermodynamics and an Introduction to Thermostatics, 2nd ed. New York, Chichester: Wiley, 1985.
17. Li ZD, Firoozabadi A. General strategy for stability testing and phase-split calculation in two and three phases. *SPE J*. 2012;17(4):1096–1107.
18. Qiu L, Wang Y, Jiao Q, Wang H, Reitz RD. Development of a thermodynamically consistent, robust and efficient phase equilibrium solver and its validations. *Fuel*. 2014;115(0):1–16.
19. Mikyška J, Firoozabadi A. A new thermodynamic function for phase-splitting at constant temperature, moles, and volume. *AIChE J*. 2011;57(7):1897–1904.
20. Mikyška J, Firoozabadi A. Investigation of mixture stability at given volume, temperature, and number of moles. *Fluid Phase Equilibr*. 2012;321(0):1–9.
21. Peng DY, Robinson DB. A new two-constant equation of state. *Ind Eng Chem Fund*. 1976;15(1):59–64.
22. Dennis JE, Schnabel RB. *Numerical Methods for Unconstrained Optimization and Nonlinear Equations*. Englewood Cliffs, NJ: Prentice-Hall, 1983.
23. Qiu L, Wang Y, Jiao Q, Wang H, Reitz RD. *Simulating Condensation in a Supercritical Gas Jet*. In: ILASS Americas, 25th Annual Conference on Liquid Atomization and Spray Systems. Pittsburgh, PA, May 5–8, 2013.
24. Qiu L, Reitz RD. Condensation processes in a motoring engine. *J Supercrit Fluids*. 2014;90(0):84–100.
25. Star AM, Edwards JR, Lin KC, Cox-Stouffer S, Jackson TA. Numerical simulation of injection of supercritical ethylene into nitrogen. *J Propul Power*. 2006;22(4):809–819.
26. Qiu L, Wang Y, Reitz RD. On regular and retrograde condensation in multiphase compressible flows. *Int J Multiphase Flow*. 2014;64(0):85–96.
27. Qiu L, Wang Y, Reitz RD. *Simulating Retrograde Condensation in a Shock Tube*. In: ILASS Americas, 26th Annual Conference on Liquid Atomization and Spray Systems. Portland, OR, May 18–21, 2014.
28. Reid RC, Prausnitz JM, Poling BE. *The Properties of Gases and Liquids*, 4th ed. New York: McGraw-Hill, 1987.
29. Firoozabadi A. *Thermodynamics of Hydrocarbon Reservoirs*. New York: McGraw-Hill, 1999.
30. Sandler SI. Chemical and Engineering Thermodynamics, 3rd ed. New York: Wiley, 1999.
31. Carroll JJ, Mather AE. A generalized correlation for the peng-robinson interaction coefficients for paraffin hydrogen-sulfide binary-systems. *Fluid Phase Equilibr*. 1995;105(2):221–228.
32. Castier M. *Private Communications*. University of Wisconsin-Madison, 2013.
33. Nishiumi H, Arai T, Takeuchi K. Generalization of the binary interaction parameter of the Peng-Robinson equation of state by component family. *Fluid Phase Equilibr*. 1988;42:43–62.
34. Grausø L, Fredenslund A, Mollerup J. Vapour-liquid equilibrium data for the systems $C_2H_6 + N_2$, $C_2H_4 + N_2$, $C_3H_8 + N_2$, and $C_3H_6 + N_2$. *Fluid Phase Equilibr*. 1977;1(1):13–26.
35. Gasem KAM, Hiza MJ, Kidnay AJ. Phase behavior in the nitrogen + ethylene system from 120 to 200 K. *Fluid Phase Equilibr*. 1981;6(3–4):181–189.
36. Amsden AA. *KIVA-3V, Release 2, Improvements to KIVA-3V*, Research report LA-13608-MS, Los Alamos National Laboratory, 1999.
37. Reitz RD, Rutland CJ. Development and testing of diesel engine CFD models. *Prog Energ Combust*. 1995;21(2):173–196.
38. Trujillo MF, O'Rourke PJ, Torres D. *Generalizing the Thermodynamics State Relationships in KIVA-3V*. Los Alamos National Laboratories, 2002.
39. Wegener PP, Mack LM. Condensation in supersonic and hypersonic wind tunnels. In: Dryden HL, Th. von K, editors. *Advances in Applied Mechanics*, Vol. 5. Elsevier, 1958:307–447.
40. Pan HQ, Firoozabadi, A. Two-phase isentropic compressibility and two-phase sonic velocity for multicomponent-hydrocarbon mixtures. *SPE Reserv Eval Eng*. 2000;3(4):335–341.
41. Nichita DV, Khalid P, Broseta D. Calculation of isentropic compressibility and sound velocity in two-phase fluids. *Fluid Phase Equilibr*. 2010;291(1):95–102.
42. Castier M. Thermodynamic speed of sound in multiphase systems. *Fluid Phase Equilibr*. 2011;306(2):204–211.
43. Robinson DB, Peng DY. The Characterization of the Heptanes and Heavier Fractions for the GPA Peng-Robinson Programs. Gas processors association;1978. Research Report RR-28.

Appendix: Equation of State

The Peng–Robinson EOS[21] was adopted to consider real gas behavior of the form

$$P=\frac{R_u T}{v-b}-\frac{a}{v(v+b)+b(v-b)} \tag{A1}$$

Here, a and b are the two parameters determined from

$$\begin{cases} a=0.457235\dfrac{R_u^2 T_c^2}{P_c}\cdot\alpha \\ b=0.077796\dfrac{R_u T_c}{P_c} \\ \alpha=\left[1+\kappa\left(1-\sqrt{T_r}\right)\right]^2 \end{cases} \tag{A2}$$

with

$$\kappa=0.37464+1.54226\omega-0.26992\omega^2 \tag{A3a}$$

An expanded formula[43] was used when ω was greater than 0.5

$$\kappa=0.3796+1.485\omega-0.1644\omega^2+0.01667\omega^3 \tag{A3b}$$

In the case of a mixture, the classical Van der Waals mixing rule was used

$$\begin{cases} a=\sum_i\sum_j x_i x_j a_{ij} \\ b=\sum_i x_i b_i \\ a_{ij}=\left(1-\delta_{i,j}\right)\sqrt{a_i}\sqrt{a_j} \end{cases} \tag{A4}$$

Manuscript received Jan. 26, 2014, and revision received June 1, 2014.